

# THE THREE-DIMENSIONAL FULLY KINETIC ELECTRO-MAGNETIC PIC SIMULATION CODE GISMO

J.-P. KUSKA AND J. BÜCHNER

*Max-Planck-Institut für Aeronomie, Max-Planck-Str. 2,  
D-37191 Katlenburg-Lindau, Germany*

**Abstract.** Since the stability of marginally thin current sheets has to be treated kinetically we have developed the three-dimensional fully kinetic electromagnetic particle-in-cell (PIC) code GISMO. Here in this paper we describe our actual simulation approach and demonstrate the possibilities of the related advanced diagnostics tools written in Mathematica and C. We illustrate some of the abilities of the GISMO package by a visualization of the results of kinetic simulations of the decay of thin current sheet. With the help of a (free) virtual reality viewer one can interactively investigate the three-dimensional structure of the unstable wave, using the enclosed CD-ROM on a PC. The temporal evolution of the instability can also be viewed using the attached CD-ROM with any WEB-browser.

## 1. Introduction

Theoretical investigations have predicted that thin current sheets usually are formed in astrophysical plasmas (Parker, 1994; Schindler, this volume). Meanwhile experimental investigations have verified the existence of thin current sheets *in situ*. Prior to substorm onsets, for example, the thickness of the current sheet in the near Earth's magnetotail reaches the order of the thermal ion gyro-radius in the ambient magnetic field  $\rho_{i0}$  and of the ion inertial length  $c/\omega_{pi}$  (Kaufmann, 1987; Mitchell *et al.*, 1990; Sergeev, 1990; Pulkkinen *et al.*, 1992; Sanny *et al.*, 1994). In such thin current sheets the non-gyrotopic properties of the particle motion with their typical meandering (Speiser) orbits across the sheet midplane becomes important. A first attempt towards an appropriate non-local linear stability theory was undertaken by Yamanaka (1978). Lapenta and Brackbill (1997) tried to calculate the dispersion properties numerically and currently we succeeded

in solving the corresponding eigenvalue problem analytically (Büchner and Kuska, 1999). It appeared that both electron and ion resonant interactions with the field of the unstably growing mode have to be taken into account (Büchner, 1998b). Appropriate numerical plasma simulations must, therefore, be kinetic, resolving both the electron- and the ion interaction with the electromagnetic fields. First attempts in this direction were reported by Winske (1981) and Brackbill *et al.* (1991). However, they just saw some gradient instability at the edges of the current sheet in the very beginning of the sheet evolution while they did not follow the sheet decay further. First results about the non-local bulk current instability of thin current sheets were published in 1996 (Büchner and Kuska, 1996; Ozaki *et al.*, 1996; Pritchett *et al.*, 1996; Zhu and Winglee, 1996). It appeared that the bulk current instability directly leads to reconnection. The questions remained open how and in which mode - symmetric sausage mode or asymmetric kink mode. We have now improved the GISMO code and developed a number of appropriate diagnostic tools to solve these and other open problems. In section 2 we describe the actual properties of GISMO and in section 3 we demonstrate some advanced diagnostics illustrating the instability of thin current sheets. On the CD-ROM attached to this volume one finds movie files demonstrating the temporal evolution of the instability. They can easily be viewed by any WEB-browser. The CD-ROM also contains virtual reality files which demonstrate the three-dimensional structure. They can be viewed interactively using a virtual reality viewer available from the WEB for free.

## 2. Simulations

GISMO is a fully kinetic electromagnetic particle- in-cell (PIC) code (Birdsall and Langdon, 1991). GISMO integrates the relativistic equations of particle motion

$$\begin{aligned}\frac{\partial v_x^*}{\partial \tau} &= \sqrt{1 - v^{*2}} \left( F_x (1 - v_x^{*2}) - F_y v_x^* v_y^* - F_z v_x^* v_z^* \right) \\ \frac{\partial v_y^*}{\partial \tau} &= \sqrt{1 - v^{*2}} \left( -F_x v_x^* v_y^* + F_y (1 - v_y^{*2}) - F_z v_y^* v_z^* \right) \\ \frac{\partial v_z^*}{\partial \tau} &= \sqrt{1 - v^{*2}} \left( -F_x v_x^* v_z^* - F_y v_y^* v_z^* + F_z (1 - v_z^{*2}) \right)\end{aligned}$$

where

$$\vec{F} = \frac{q}{mc^2} \left( \vec{E} + \vec{v}^* \times \vec{B} \right). \quad (1)$$

and  $\vec{v}^* = \vec{v}/c$  and  $\tau = \ell t/c$  with the maximum simulation box dimension  $\ell = \max\{\ell_x, \ell_y, \ell_z\}$ . The electromagnetic fields are obtained by solving the wave equations for the scalar and vector potentials  $\phi$  and  $\vec{A}$

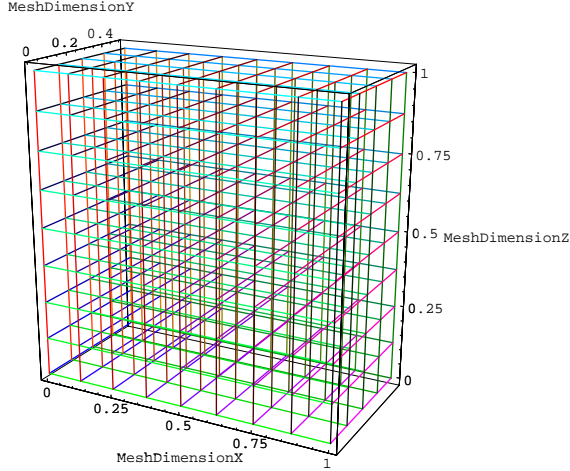


Figure 1. Example of a rectangular three-dimensional mesh for the potentials.

$$\Delta\phi - \frac{1}{c^2} \frac{\partial^2 \phi}{\partial t^2} = -4\pi\rho \quad (2)$$

$$\Delta\vec{A} - \frac{1}{c^2} \frac{\partial^2 \vec{A}}{\partial t^2} = -4\pi\vec{j} \quad (3)$$

In order to save computer time at any time step the potentials and fields are determined at any grid point of a three-dimensional mesh, shown in Fig. 1, using the Lorenz gauge condition

$$\frac{1}{c} \frac{\partial \phi}{\partial t} + \vec{\nabla} \cdot \vec{A} = 0. \quad (4)$$

For solving the equations of motion (1) the field values are trilinearly interpolated between the neighbouring grid points. The description of the potentials by wave equations has several advantages. The most notable one is the easy implementation of an implicit integration scheme and the simple formulation of the boundary conditions. The integration of the wave equation

$$\frac{\partial^2 w}{\partial t^2}(x, y, z, t) = \Delta w(x, y, z, t) + S(x, y, z, t) \quad (5)$$

is performed by the scheme

$$\begin{aligned} \frac{1}{h_0 + h_1} \left( \frac{w^{(n+1)} - w^{(n)}}{h_0} - \frac{w^{(n)} - w^{(n-1)}}{h_1} \right) = \\ \frac{1}{2} \left( \Delta w^{(n+1)} + \Delta w^{(n-1)} \right) \\ + \frac{1}{2} \left( S^{(n+1)} + S^{(n-1)} \right) \end{aligned} \quad (6)$$

with  $h_0 = t^{(n+1)} - t^{(n)}$  and  $h_1 = t^{(n)} - t^{(n-1)}$ . This scheme is implicit and unconditionally stable for all step sizes  $h_n$ . GISMO carries out a step size adjustment by the particle integrator. The Laplacian for solving the wave equation (5) is approximated by the finite difference expression

$$\begin{aligned} \Delta w^{(n)}(x, y, z) \approx & \frac{w_{i+1,j,k}^{(n)} - 2w_{i,j,k}^{(n)} + w_{i-1,j,k}^{(n)}}{\delta x^2} \\ & + \frac{w_{i,j+1,k}^{(n)} - 2w_{i,j,k}^{(n)} + w_{i,j-1,k}^{(n)}}{\delta y^2} \\ & + \frac{w_{i,j,k+1}^{(n)} - 2w_{i,j,k}^{(n)} + w_{i,j,k-1}^{(n)}}{\delta z^2} \end{aligned} \quad (7)$$

where  $\delta x$ ,  $\delta y$  and  $\delta z$  are the grid distance in the three spatial directions. The time discretisation scheme (6) yields, together with the approximated Laplacian given by equation (7), a sparse linear system of equations for the  $w_{i,j,k}^{(n+1)}$ . This set of equations is solved at every time step by successive over-relaxation with a conjugate gradient preconditioner. The iterative solution is started with the potential of the previous time step, usually the initial guess for  $w^{(n+1)}$  is very close to the solution only a few iterations are needed to obtain the desired accuracy. Electric and magnetic fields are calculated from the potentials by finite difference expressions for the derivatives. The continuous electric and magnetic fields are obtained by a trilinear interpolation of the data between the mesh points. Notice that the particle motion across the boundaries of the simulation box violates the gauge condition. The forces are, therefore, corrected as soon as the error in the gauge equation (4) exceeds the error in the iterative solution of the wave equation. Both the charge  $\rho$  and the current density  $\vec{j}$  are calculated from the positions and velocities of the particles. The solution of the relativistic equations of motion (1) is obtained using an explicit embedded Runge-Kutta scheme of the order 4(3) with step size control (Deuffhard, 1994). This is the classical Runge-Kutta method but with an embedded third order step. Table 1 provides the coefficients which we used for the integration of the particle

0					
1/2	1/2				
1/2	0	1/2			
1	0	0	1		
1	1/6	1/3	1/3	1/6	
$\xi$	1/6	1/3	1/3	1/6	0
$\xi^*$	1/6	1/3	1/3	0	1/6

TABLE 1. Butcher tableau used for the integration of the particle orbits.

orbits. The fourth order integration scheme ensures that the particle gyration in the magnetic field is resolved properly. The step size control plays an important role in the integration of the equations of motion. In fact, the accuracy of the integration is an often overlooked quantity in kinetic simulations. However, the correct modeling of the dynamic system usually requires a stable *and* accurate solution, with the accuracy being even more important! The step size control ensures both that the solution stays stable and that the local truncation error

$$[\hat{\epsilon}] = (\xi - \xi^*)/6 \quad (8)$$

is lower than the desired accuracy for all trajectories (here  $\xi$  and  $\xi^*$  are the fourth and third order approximation obtained by the embedded Runge-Kutta pair). For modeling an instability the step size control speeds up the calculation during the initial metastable phase of the system evolution and the classical Runge-Kutta method has the advantage that it can be implemented in a memory efficient way. In addition to the memory saving implementation the classical Runge-Kutta method contains two redundant steps in the middle of the integration interval  $h$  and at the end. This redundancy improves the convergence of the solution for the particle motion. Higher order Runge-Kutta integrators (Cash and Karp, 1990; Hairer et al., 1987; Verner, 1993) would not improve the integration quality due to the force term, calculated by a low order interpolation. The maximum local error of the integration was chosen to be  $\hat{\epsilon} < 1 \cdot 10^{-5}$ . The motion of the particles near boundaries must be consistent with the boundary conditions for the fields. In the case of a Harris (1962) equilibrium we assume, for example, periodic boundary conditions in the  $x$  and  $y$  directions  $0 \leq x \leq \ell_x$ ,  $0 \leq y \leq \ell_y$ ,  $0 \leq z \leq \ell_z$  box, i.e.  $w(0, y, z) = w(\ell_x, y, z)$  and  $w(x, 0, z) = w(x, \ell_y, z)$ . Further we put the potentials to zero at the upper and lower boundaries and use free boundary conditions in the remaining directions.

### 3. Diagnostics

Here we want to draw the readers' attention to the unavoidable necessity and essential importance of appropriate and advanced diagnostic tools. This is especially important in case of three-dimensional particle code simulations due to the vast amount of data produced. High quality diagnostics must be able to organize the simulated data output in a way that allows a most direct verification or falsification of hypotheses based on theoretical or experimental investigations. We will demonstrate this by using the instability of thin current sheets as an example. The linear dispersion theory of thin current sheets predicts a most unstable density wave propagation in the current direction. For small mass ratios the wavelength should depend on it, with  $\lambda \approx 2\pi L_z$  for a mass ratio  $M = 1$  and  $\lambda \approx 2L_z$  for  $M = 64$ . The oscillation frequency is expected to be close to the ion frequency in the ambient magnetic field (Büchner and Kuska, 1999). The mode should also couple to reconnection with a wave vector  $k_x$  perpendicular to that of the unstable wave ( $k_y$ ). The recognition of such mode calls for a three-dimensional diagnostics in the real space. In the velocity space one could investigate the responsible resonant interactions. Also, everything should be presented in its time dependence, since the process is dynamic, non-stationary. As an example we demonstrate part of our diagnostics for runs, simulating the unstable decay of thin (Harris, 1962) -type current sheets. The runs were carried out on a  $128 \times 128 \times 64$  mesh for the electromagnetic potentials. The box sizes were chosen as  $12L_z \times 12L_z \times 6L_z$  in physical units with  $L_z$  being the sheet half-width. In our example the simulation parameters were  $T_e = T_i = 40 \text{ keV}$ ,  $u_{di} = 2 v_{ti}$  and  $n = 1 \text{ cm}^{-3}$ . This parameter set guarantees both a thin current sheet and a sufficiently high resolution of the Debye length. The temporary evolution of the sheet can be followed best by watching the movies, stored on the attached CD-ROM. For comparison we show results for a mass ratio  $M = M_i/m_e = 1$  and for  $M = 64$ . The three-dimensional structure can be viewed using the virtual reality files, also stored on the attached CD-ROM. They were produced for three different moments of time. The virtual reality approach allows to see the density structures from all possible view angles. We show one particular snapshot out of them in Fig. 2. The Figure corresponds to a moment of time after a sausage mode bulk current instability has developed. Fig. 2 depicts the ion density isosurface for a mass ratio  $M = 64$  simulation. In addition the left wall of the box shows isodensity contours for a cut through the box at  $X = 6 L_z$ . At the bottom one sees isodensity contours for a cut through the box at  $Z = 3 L_z$ . This specific view angle allows to watch the transition to three-dimensional reconnection, as discussed in more details in a separate paper (Büchner, this volume).

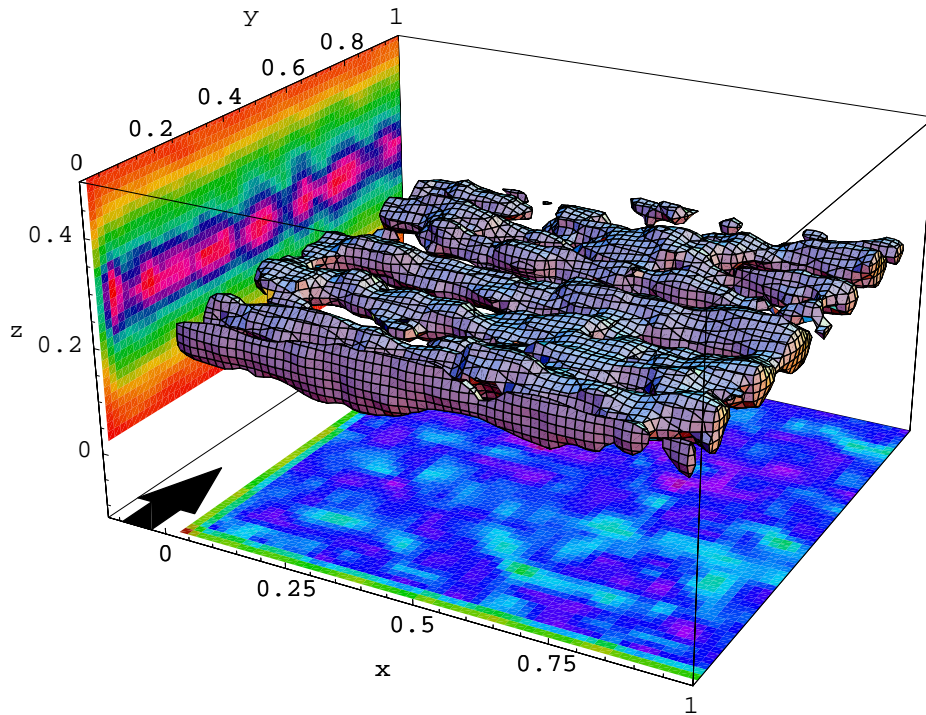


*Figure 2.* Example for the advanced GISMO-diagnostics tools based on Mathematica and C: Ion density isosurface for a developed sausage mode instability in case of a mass ratio  $M = 64$ . The left box side shows isodensity contours for a cut through the simulation box at  $X = 6L_z$  and the bottom plane depicts isodensity contours for a cut through the box at  $z = 3L_z$  can be seen. The arrow indicates the current and wave propagation direction

#### 4. Conclusion

Since we published in 1996 the first simulation results obtained by the newly developed GISMO code, we have developed its performance further and, mainly, added a large number of diagnostic tools based on Mathematica and C. Now GISMO has proven to be a stable and flexible program for kinetic plasma simulations. A number of physical results was already obtained or illustrated by using GISMO (cf., e.g., Büchner and Kuska, 1996; Büchner and Kuska, 1999; Büchner and Kuska, 1997; Büchner *et al.*, 1998a; Büchner, 1998b). The stability of GISMO is due to the implemented step size control scheme and other original features described in this paper. Its flexibility arises from the usage of C-WEB TCL scripts for controlling the program. This allows an easy extension of GISMO to simulate other plasma problems where both electron and ion interactions are important.

## References

- Birdsall, C.K. and Langdon, A.B., *Plasma Physics via Computer Simulation* Plasma Physics Series. IOP Publishing, 1991.
- Brackbill, J.U., D.W. Forslund, K.B. Quest, and D. Winske, Nonlinear evolution of the lower-hybrid drift instability, *Phys. Fluids*, *27*, 2682, 1984.
- Büchner, J., and J.-P. Kuska, Three-dimensional collisionless reconnection through thin current sheets: Theory and selfconsistent simulations, in *Proceedings of the IIIrd International Conference on Substorms, ESA SP - 389*, October 1996, 373, 1996.
- Büchner, J., and J.-P. Kuska, Numerical simulation of three-dimensional reconnection due to the instability of collisionless current sheets, *Adv. in Space Res.*, *19*, 1817, 1997.
- Büchner, J., et al., Three-dimensional reconnection in the Earth's magnetotail, in *Geophysical Monograph*, *104*, 313, 1998a.
- Büchner, J., Kinetic effects controlling the onset of 3D tail reconnection, in *Substorms-4*, eds. S. Kokubun and Y. Kamide, Kluwer Academic Publishers, pp 461, 1998b.
- Büchner, J., and J.-P. Kuska, Bulk current instability through thin current sheets, *Annales Geophys.*, *103*, 1999 (in press).
- Cash, J. R. and Karp, A. H. A variable order Runge-Kutta method for initial value problems with rapidly varying right-hand sides, *ACM transactions on Mathematical Software*, Vol. *16*, 201, 1990.
- Deuffhard, P. and Bornemann, F., *Numerische Mathematik II: Integration gewöhnlicher Differentialgleichungen*, Verlag de Gruyter, Berlin, 1994.
- Hairer, E., Norsett, S. P., and G. Wanner, *Solving Ordinary Differential Equations I. Nonstiff Problems*, *Springer Series in Computational Mathematics 8*, Springer-Verlag, 1987.
- Harris, E.G., On a plasma sheath separating regions of oppositely directed magnetic field, *Nuovo Cimento*, *23*, 115, 1962.
- Kaufmann, L.R., Substorm currents: Growth phase and onset, *J. Geophys. Res.*, *92*, 7471, 1987.
- Lapenta, G., and J.U. Brackbill, A kinetic theory for the drift-kink instability, *J. Geophys. Res.*, *102*, 27099, 1997.
- Mitchell, D.G. et al., Current carriers in the near-Earth's cross-tail current sheet during a substorm growth phase, *Geophys. Res. Lett.*, *17*, 583, 1990.
- Ozaki, M., Sato, T., Horiuchi, R., and CS Group, Electromagnetic instability and anomalous resistivity in a magnetic neutral sheet, *Phys. Plasmas*, *3*, 2265, 1996.
- Parker, E., *Spontaneous Current Sheets in Magnetic Fields*, Oxford Univ. Press, New York, NY, 1994.
- Pritchett, P.L., F.V. Coroniti and V.K. Decyk, Three-dimensional stability of thin quasi-neutral current sheets, *J. Geophys. Res.*, *101*, 27,413, 1996.
- Pulkkinen, T. et al., Particle scattering and current sheet stability in the geomagnetic tail during the substorm growth phase, *J. Geophys. Res.*, *97*, 19,283, 1992.
- Sanny, J., R.L. McPherron, C.T. Russell, D.N. Baker, T.I. Pulkkinen, and A. Nishida, Growth-phase thinning of the near-Earth current sheet during the CDAW 6 substorm, *J. Geophys. Res.*, *99*, 5805, 1994.
- Sergeev, V., et al., Current sheet thickness in the near-Earth plasma sheet during substorm growth phase, *J. Geophys. Res.*, *95*, 3819, 1990.
- Verner, J. H., Differentiable interpolants for high-order Runge-Kutta methods, *SIAM J. Numer. Anal.*, *30*(5), 1446, 1993.
- Winske, D., Current-driven microinstability in a neutral sheet, *Phys. of Fluids*, *24*, 1069, 1981.
- Yamanaka, K., Threshold of electromagnetic instability in a magnetic neutral sheet, *Physica Scripta*, *17*, 15, 1978.
- Zhu, Z., and R.M. Winglee, Tearing instability, flux ropes, and the kinetic current sheet kink instability, *J. Geophys. Res.*, *101*, 4885, 1996.